# *Review of Literature*

# CHAPTER II

# REVIEW OF LITERATURE

This chapter discusses a brief review about the research works carried out in the context of the design and development of an air assisted sprayer with electrostatic nozzle for coconut palms.

## 2.1 MORPHOLOGICAL CHARACTERISTICS OF COCONUT PALM

Coconut palm (*Cocos nucifera L.*), one of the major tropical crops, belongs to the *Aceraceae* family and the genus Cocos. The plant is also one of the largest monocotyledon plants. It is an important perennial crop grown in more than 80 countries, with the major shares coming from the Philippines, India, Sri Lanka, and Indonesia (Chan and Elevitch, 2006; Arunachalam, 2012). It is believed that the crop evolved from the region encircling the Bismarck Archipelago, New Guinea, and the Malaysian Peninsula, from where it spread throughout the tropics. Coconut farming has been practiced in India for more than three millennia, especially throughout the southern margin of the Indian subcontinent. The crop is inextricably intertwined with Kerala's economic prosperity and sociocultural heritage, just like in other coconut-growing regions across the globe. The crop is also known as the "Tree of Life" or "Kalpavriksha" because of the incredible variety of goods and services provided by the tree. It is advised to plant tall, dwarf, and hybrid varieties in a 60:20:20 ratio for the sustainable growth of coconut sector. However, actual situation under field level has more than 90 per cent of tall variety (Thamban *et al.,* 2016; Ignacio and Miguel, 2021; Kumar and Kunhamu, 2022).

The plant has a single, unbranched trunk with a symmetrical canopy with oval or round fruits (Gilman and Watson, 1993; Chan and Elevitch, 2006). The stem is typically erect, pillar like with a swollen base called 'bole'. The plant can attain heights of 20–22 meters in 40 years, and 35–40 meters in 80 years, with a canopy span of about 8–9 meters. The growing part is located at the centre of the top stem. The cylindrical stem is surrounded by a band of tissue (cortex) called bark. The thickness of bark is

generally 10 mm and is thicker at the bottom. The surface of the cortex has leaf scars in a triangular shape. The distance between the leaf scars gives the growth rate of the palm. All the leaves are growing from the stem apex. The newly formed leaves are curved and wrapped together to form the heart of the palm. The oldest leaves are located at the lowest whorls, depending on the palm variety and growing conditions (Chan and Elevitch, 2006; KAU, 2019).

The plant consists of an unbranched crown of large leaves, called fronds, are generally even-pinnate or paripinnate in nature, located at the top of the trunk with a spread in the range of 4.5 to 7.6 m (15 to 25 feet) (Chan and Elevitch, 2006; Gilman and Watson, 1993; Pham, 2016). The oddly pinnately compound-type leaves are arranged in a spiral pattern around the tree trunk. Each leaf consists of 200 to 250 linear leaflets arranged on both sides of the rachis in a single plane. A single leaflet is 0.5 to 1.5 m long and 15 to 50 mm wide. A single frond can be 1.5 to 5 m long, with a petiole making up a quarter of this length (Chan and Elevitch, 2006). A mature palm crown generally has 3 to 40 paripinnate leaves, with each leaf being 5 to 6 m long and 10 to 15 kg in weight. For a single leaf, the time from leaf emergence to shedding is between 2.5 and 3 years. In a healthy palm, a fresh leaf develops in the crown every three to four weeks. An average of 12 leaves are produced annually by the palm. The inflorescence grows inside a spathe, a robust, hardy, double-pointed sheath. The entire structure is called "spadix" when the spathe has fully formed and measures roughly 1 to 1.2 m in length and 140 to 160 mm in diameter. The inflorescence has 30 to 35 spikelets that contain flowers, mainly a dense cluster of male flowers. Each spikelet has 250 to 300 male blooms. The female flowers are located at the foot of the spikelet, and each spikelet may contain one or more female flowers. Each fruit will mature in 12 months (Pham, 2016; KAU, 2019).

The coconut palm has two main habitual forms namely tall and dwarf. Almost all the current varieties of coconut palm are derived from one species called *C. nucifera*. Tall varieties, like West Coast, Jamaican, and East Coast, are heterogenous due to cross-pollination, have lengthy internodes, and late-bearing stems. They reach towering heights of 20 to 30 meters and produce large fruits primarily used for oil extraction. In

contrast, dwarf varieties such as Fiji, Malayan, Macapuno, Brazilian Green, and Cameroon Red are homogenous, self-pollinated, have early-bearing stems, and attain heights of 10 to 15 meters. Hybrid varieties are developed by combing the tall and dwarf varieties, which can give early-bearing, high-yielding intermediate forms with medium-long inter-nodes (Arunachalam, 2012; Ignacio and Miguel, 2021).

Tall coconut varieties mostly produce a swollen base stem (root bole) and have relatively larger crowns. They naturally crosspollinate, producing populations and individuals that are heterozygous. They have a long gestation period of 6 to 10 years. And, once flowering begins, the process of non-seasonal nut production continues. The major tall varieties grow up to a height of 15 to 24 m. Compared to the dwarf varieties, tall varieties have a long life; under favourable circumstances, they can live more than 60 years. The annual leaf production for tall variety is ranging between 12 and 18. The tall variety of palm can have 7 m long leaves with an area of 10 $m^2$ and weigh up to 20 kg when green (Chan and Elevitch, 2006; Suriya, 2016; KAU, 2019). The fruit from tall varieties is generally medium to large in size and is predominately used for oil production (Ignacio and Miguel, 2021).

Manjula *et al.* (2014) studied the morphological characteristics of coconut palms growing in Kerala. The study was conducted on 400 plants, of which 200 were West Cost Tall (WCT) varitey growing in the coastal regions of Kasaragod district and 200 were Kuttiyadi ecotype varitey growing in the hilly regions of Kozhikode district. The palms selected are aged between 40 and 50 years. The palm height and girth at the base of the WCT and kuttiyadi varieties were 12.3 and 15.5 m and 1.02 and 1.1 m, respectively. The length of the petiole for WCT and kuttiyadi varitey was observed as 1.08 m and 0.7 m, respectively. The length of the leaflet-bearing portion in WCT is 3.43 m, whereas in Kuttiyadi it was observed as 3.42 m. The WCT variety can have an average of 112 leaflets per leaf, each with a length of 1.16 m and a width of 56.3 mm. In the kuttiyadi variety, the average number of leaflets per leaf is 111, each having a length of 1.1 m and a width of 54.7 mm. It was also observed that the number of leaf scars per metre of length was higher for WCT (14.06) compared to the kuttiyadi variety (11.59). The number of leaf scars per metre of length actually denotes the number of

internodes per metre of length. The widely spaced internodes indicate the long drooping habit, whereas the closely spaced internodes denote the well-oriented, strong, and short leaves.

The common dwarf varieties can grow up to a height of 5 to 18 m. The dwarf varieties do not produce a swollen base stem and mostly have smaller crowns. Due to the overlap of the male and female parts of the same inflorescence, they spontaneously self-pollinate, producing homozygous individuals and pure line populations. After 3 to 5 years of post-germination, these varieties produce fruits of smaller size, which are generally used for dessert production and as a source of coconut water. Dwarf coconuts have a shorter lifespan, and the delay in inflorescence emission during unfavourable environmental conditions makes their nut output seasonal. The annual leaf production for dwarf variety is about 20 to 22 (Chan and Elevitch, 2006; Suriya, 2016; KAU, 2019; Ignacio and Miguel, 2021).

The hybrid varieties generally produce nuts of intermediate size but in larger numbers than the parent plant. They are also more pest and disease resistant compared to their parent plants. The hybrid varieties begin flowering 3–6 years after planting (Ignacio and Miguel, 2021). Niral *et al.* (2019) reported on different hybrid coconut varieties developed and released by the Central Plantation Crops Research Institute (CPCRI), Kasaragod. The first coconut hybrid variety was developed in India in 1934 by Dr. J.S. Patel by cross breeding the West Cost Tall (female) and Chowghat Green Dwarf (male). Chandra Sankara, Chandra Laksha, Kera Sankara, Kalpa Samrudhi, Kalpa Sankara, and Kalpa Sreshta are major hybrid varieties. Most of the hybrid varieties are a cross-breed of a tall and a dwarf variety of coconut pam. Almost all the varieties have justation period of 4 to 5 years. Among the different hydrid varieties, Kalpa sankara varitey is tolerant to wilt disease and can attain a height of 4.98 m in 18 years. The hybrid variety Kalpa Sreshta can reach a height of 10.05 m in 23 years.

## 2.2 PEST AND ITS MANAGEMENT STRATEGIES

Coconut palms (*Cocos nucifera*) are susceptible to various pests that can impact their health and productivity. Effective pest management strategies are crucial to

mitigate the damage caused by these pests. The potential productivity of coconut palm in Kerala in the mid-2010 was 150 nuts per palm per year, however the actual yield obtained as only 40 nuts per palm per year (GOK, 2021), which clearly indicating an alarming decrease in the yield of about 275 per cent. Occurrences of diseases like root wilt, bud rot, dominance of marginal and small land holdings, attack of pest like red palm weevil, whiteflies, eriophyid mite, rhinoceros beetle, unavailability of adequate and high yielding plant varieties, lack of skilled labours and short supply of irrigation water are the major factors responsible for the low coconut productivity in Kerala (George and Kuruvila, 2022; Thamban *et al.*, 2016).

Suriya, 2016 reported that the leaves, crown, or nuts of coconut palms are frequently attacked by numerous serious pests. The two most common pests attacking coconut leaves are the coconut caterpillar (*Opisina arenosella*) and the coconut leaf beetle (*Brontispa longissima*). At the seedling stage and young bearing palm stage, two bugs, namely the black beetle (*Oryctes rhinoceros*) and the red weevil (*Rhynchophorus ferrugineus*), harm the growth point of the coconut palm, which may eventually result in the death of the palm if not timely treated. It is well known that eryophyid mites (*Aceria guerreronis*) seriously harm developing nuts, especially in plantations in arid regions of several nations that grow coconuts, such as Oman, India, and Sri Lanka.

Inavasive pests including the coconut eriophyid mite (*Aceria guerreronis*), Asian grey weevil (*Myllocerus undatus*), inflorescence moth (*Batrachedra arenosella*), and spiraling whitefly (*Aleurodicus dispersus*), which posed significant threats upon their initial introduction. Such invasive pests not only cause initial outbreaks but also risk imposing quarantine restrictions on coconut exports, impacting international trade (Mohan *et al*., 2017). The Rugose Spiralling Whitefly (RSW) exhibits a broad host range, encompassing palms, woody ornamentals, and fruit trees such as mango (*Mangifera indica*), gumbo limbo (*Bursera simaruba*), and coconut (*Cocos nucifera*). It has been documented on several palms, including areca (*Dypsis lutescens*) and *Veitchia* species, with the potential for additional hosts to be identified. RSW cause stress to the host plant by removing nutrient and water content and also by producing honeydew, a sugary fluid, which lead to the growth of sooty mold. These stress lead to

the reduction in photosynthetic efficency, defoliation and dieback of branches (Elango *et al*., 2020).

The morphological stages of RSW exhibit distinct characteristics. Eggs are laid in spiral patterns on leaf undersides, covered with white wax, appearing creamy white to dark yellow. The nymphal stage includes four immobile instars following the mobile crawler stage, which uses needle-like mouthparts to feed on sap. Nymphs are light to golden yellow in colour and produce cottony wax and filaments as they mature. The pupal stage is marked by a rugose vasiform orifice, spinulose operculum, and specific pore and setae patterns. Adults are three times larger than common whiteflies, with distinctive light brown wing bands, and males have pincer-like abdominal structures (Elango *et al*., 2020).

Managing RSW is challenging due to its wide range of wild host plants that support pest buildup. Integrated Pest Management (IPM) aims to control pests economically and ecologically by combining resistant varieties, cultural, physical, mechanical, biological, and chemical strategies, minimizing pesticide use. Key IPM practices include monitoring, sampling, and record-keeping to maintain pest levels below economic thresholds. Yellow sticky traps are widely used for monitoring and managing whiteflies, with studies showing a strong correlation between trap catches and field populations. Biological control, involving natural enemies, is a preferred method for managing RSW. This approach, combined with systemic insecticides, offers potential for effective management (Taravati *et al*., 2013).

## 2.3 EQUIPMENT FOR SPRAYING CHEMICAL PESTICIDES ON COCONUT PALMS/TALL TREES

Manian *et al.,* 2002 developed a tractor operated sprayer suitable for coconut trees. The developed sprayer unit consists of 8 to 14 m long telescopic pole made of G.I. pipe, tractor Power Take Off (PTO) Shaft operated pump, two spray guns and a chemical reservoir. The spray guns were mounted on the top of a telescopic pole, which can extend up to 9 to 14 m in such a way that the two guns can be moved up and down using a rope arrangement from the ground level. The optimum angle of inclination from

the horizontal at maximum height of reach (6.92 m from the nozzle tip) was observed as 75º. It was also observed that the height of reach was reduced to 5.10 m when the two spray guns were operated simultaneously. The entire system can be fold and kept in horizontal position while transportation and can erect vertically during the operation. The unit can spray about 35 palms per hour depending on the height and canopy distribution. It is also suitable for other tall trees and orchards.

Samseemoung *et al.* (2017) designed and developed a spraying system for coconut plantations. The unit consists of a power system, motor, pump, chemical storage tank, a nozzle equipped with remote monitoring system, a crane and motion controlling system. The location of the infected pest is identified through the image processing system. And then the spraying is done by moving the crane towards the detected location by means of remote monitoring system. The evaluation was done for 5 to 9 m tall coconut trees. The nozzle–target distance was 1 m, with the spraying rate of 2.72 $L \cdot min^{-1}$ at an operating pressure of 1.5 bar. The field capacity was observed as 0.056 $ha \cdot h^{-1}$ with fuel consumption of 0.58 $L \cdot min^{-1}$.

Kumar *et al.* (2018) conducted the performance evaluation of front mounted power tiller operated tall tree sprayer, consists of a main frame, pump operated by the power tiller, power transmission system, spray booms and chemical tank. The pump pulley of 300 mm diameter was connected to the engine pulley of 100 mm diameter through a belt (B-48). The results showed that, at a pressure of 3.5 $kg \cdot cm^{-2}$, the spray cross-section area (3421.20 $cm^2$) and included angle of nozzle (92.66º) became stable. The discharge rate was found directly related to the pressure. The optimum discharge of 706 $mL \cdot min^{-1}$ was observed at 3 $kg \cdot cm^{-2}$ pressure. The maximum height of reach was 7.2 m for tall trees. The working capacity was 80 trees per hour with fuel consumption of 0.636 $L \cdot h^{-1}$.

Sanjay and Jeevitha (2023) developed a Hexa-copter type agriculture drone for the disease detection and pesticide application for coconut palms. The drone has an image processing camera conjoined with machine learning techniques for the detection of the accurate location of infected area and simultaneous spraying of pesticides through

the spray nozzles. The system consists of transmitter-receiver arrangement, gyroscope sensors, motor and accelerometer to control the flight motion. The spraying unit consist of Li-Po battery, pump, storage tank, and nozzles. Whereas the image acquisition unit consists of a First-Person View (FPV) camera which powered by the current from the flight controller. The drone can effectively apply pesticides/insecticides to the crown and other areas of the coconut tree. Spray application rates were observed as ranging between 10 and 50 $L \cdot ha^{-1}$ by modifying the effective swath width and flight patterns.

## 2.4 APPLICATION OF ELECTROSTATICS IN PRECISION SPRAYING

The electrostatic method of spraying involves the application of spray droplets, superimposed with electric charge, while the target is grounded. The working principle of the system is based on Coulomb's law. The electrically neutral droplets released from the nozzle were charged electrostatically, which disturbs its normal balance. The complex process of electrostatic spraying can be subdivided into three in which the first stage of liquid atomization and droplet charging, transport of the charged droplets through the atmosphere (trajectory), and the deposition of charged droplets on the target by means of electrostatic force (Chigier, 2006; Mamidi *et al.,* 2013; Patel, 2016; Appah *et al.*, 2019).

### 2.4.1 Droplets in electric field

Many researches have been conducted to explain the atomization mechanism of water-based droplets in electric field. The two general and fundamental theory for the disintegration droplets in the electrostatic field are: (1) The electrostatic spraying process can be considered as an equilibrium end-state problem; (2) It is a random complex process involving ample number of droplets and charge. The first being popularly accepted. The later statement implies the observation in which, the droplets are randomly formed at the spray tip under the high voltage conditions (Kelly, 1978).

The surface tension and viscous shearing resistance of liquid are the major two resistance to be overcome for the electrostatic atomization of liquids. (Hines, 1966; Gomez and Tang, 1994; Zheng *et al.,* 2002). Surface tension offers the major resistances

for the electrostatic atomization, particularly for water-based liquids with dipole moments. When an external electric field is applied, liquid molecules undergo a rearrangement, shifting from their static isotropic orientation to the dipole alignment parallel to the applied electric field. This rearrangement reduces the force of interaction between liquid molecules, consequently lowering surface tension. This decrease in surface force induced by the electric field can be quantified by comparing surface tension values before and after its application. When the electrostatic force overcomes the surface tension, the droplet breaks. This unstable condition is termed as *Coulomb fission.* During this time, the liquid meniscus forms a conical shape at the capillary outlet and may disrupt along the cause of low resistance (O'Konski and Thacher Jr, 1953; Taylor, 1964; Zheng *et al.*, 2002; Gu *et al*., 2007)

The fine charged droplets formed by the disintegration of large droplets or stream may then move forward under the influence of air stream and other forces acting on the droplet. As the charged droplet approaches the earthed target, it builds up charge on the target surface. The electrostatically charged target may have charge opposite to that of the droplets. As the principle that opposite charge attracts (Coulomb's law) droplets gets supplementary force to move towards the target (Matthews, 1989; Singh *et al.*, 2013; Appah *et al.*, 2019). As the droplet move closer to the target, the effect of electric field force ($F_e$ = qE) declines. Whereas the effect of gravitational and electrostatic force between the target and the droplet may shoot up (Zheng *et al.*, 2002). By virtue of the electrostatic attraction, the droplets may settle on both abaxial and adaxial sides of the target (Laryea and No, 2003; Patel *et al*., 2013). Immediately after each target has been sufficiently covered with the spray solution, the target loses its charge and spray charge can move to next surfaces that has to be covered (Matthews, 1989; Singh *et al.*, 2013; Appah *et al*., 2019).

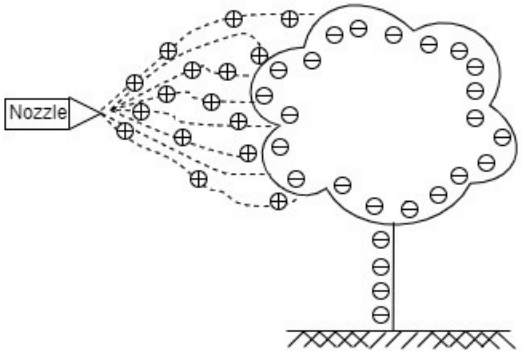


**Figure 1. Charged droplets moving towards the target** (Zheng *et al.,* 2002)

### 2.4.2 Charge acquisition methods

Several charging methods can be employed for the driving electric field of the electrostatic spraying including induction charging of conductive liquids, ionized charging (corona charging) of either conductive or non-conductive liquids, and direct charging of low or semi-conductive liquids, with the first one being predominant (Law, 1978; Matthews, 1989).

#### *2.4.2.1 Induction charging*

Induction charging method is the most convenient and practical method for the electrification of droplets and is suitable for conductive liquids. This method of charging consisted of an electrode which is connected to a high voltage supply placed adjacent to the grounded spray charge as shown in Figure 2.

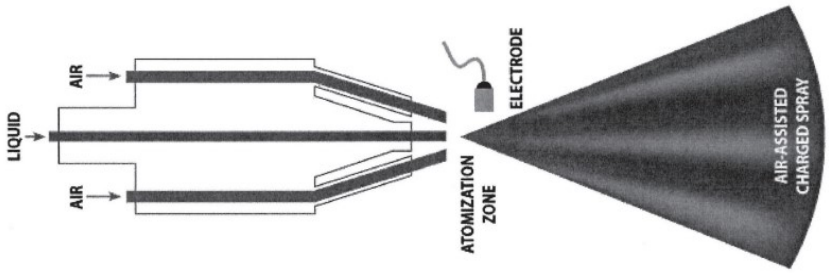


**Figure 2. Induction charging (Singh *et al*., 2013)**

The negatively charged electrode can induce a positive charge on the conductive liquid and vice versa and a portion of these charge may retain when they broke down into droplets (Law, 1978; Marchant and Green, 1982; Matthews, 1989). The charge induced per unit area depend upon the electrode voltage and conductivity of the material to be charged (Matthews, 1989). The general voltage requirement is in the range of 5–15 kV for the liquids of electrical conductivity ranging from $10^4$ to $10^6$ ohm (Toljic *et al.*, 2008; Singh *et al.*, 2013).

*2.4.2.2 Ionized field charging or corona charging*

This method has been considered as the most difficult due to the charge leakage problems, fragile nature of the electrode, higher ionization voltage requirements, chances of reverse ionization, and safety concern. Ionized field or corona charging method consisted of a sharp-needle electrode held at a very high voltage potential. The applied high voltage builds up an intense electric field around the needle electrode ionizes the surrounding air. The positively charged electrode will repel the positive ions and the negatively charged ions that attracts back may neutralize some of its charges. The reverse is true for the negatively charged electrodes. The charged ions are then carried away by the liquid droplets as they pass through the near vicinity of the electrode tip. The level of charge is depended on the time, surface area, dielectric constant of the liquid, and the electrical characteristics of the corona discharge. The voltage requirement is in the range of 30 to 130 kV. This method is more suitable for liquids with wide range of conductivity and for purposes like dry powder coating, precipitations of smoke and dust (Law, 1978; Marchant and Green, 1982; Matthews, 1989; Law, 2014; Khatawkar *et al.*, 2021).

*2.4.2.3 Direct charging*

In direct charging or contact charging, the charging is achieved by the conductive method as the liquid comes in direct contact with an electrode held at high voltage (15-40 kV). Semi-conductive liquids having electrical resistivity ranging between $10^4$ to $10^6$ ohm·m can be charged by this method. The direct contact between the liquid coming out through narrow opening and the high voltage electrode causes a

mutual electric repulsion among the distinct portions of the charged liquid, which breaks the surface tension to form small droplets. This method of charging is more suitable for oil-based than water-based liquid as the evaporation of the small droplets is a serious concern with later one (Matthews, 1989; Singh *et al.*, 2013; Law, 2014; Khatawkar *et al.*, 2021).

### 2.4.3 Electrostatic spraying for plant protection

Researchers have explored various electrostatic spraying system parameters for pesticide application. The system electrostatic spraying for agriculture application consists of many components, whose optimal selection will help to achieve the most effective spraying.

Law (1983) developed electrostatic sprayer consisting of a pneumatic nozzle and charging of liquid is achieved by an induction electrode. This system demonstrated a 2-to-7-fold improvement in the effectiveness of droplet deposition compared to conventional spraying methods. Laryea and No (2003) has come up with a pressure-swirl nozzle for electrostatic spraying, which was capable of efficiently spraying pesticides at a low application rate, ensuring maximum deposition while minimizing droplet drift to non-target substrates. Ru *et al*. (2008) developed an axial flow air-assisted ultra-low volume electrostatic sprayer equipped with a high voltage (20 kV) corona charging system. Celen *et al*. (2009) developed a tunnel type air assisted electrostatic sprayer. The tunnel system prevents spray drift and unwanted adhesion. Mamidi *et al.* (2013) developed an electrostatic hand pressure knapsack sprayer with two swirl discs with 1 mm swirl hole diameter and an orifice disc with 0.8 mm diameter hole. Patel *et al*. (2017) developed a novel air-assisted electrostatic nozzle suitable for small-scale farms. Dai *et al*., (2022) developed an electrostatic spray system with an air-assisted electrostatic nozzle. These results concluded that, the air assistance while spraying enhances droplet penetration into the plant canopy, whereas the electrostatic system improves droplet adhesion.

Law (1978) done the theoretical analysis of spray droplet charging using a completely embedded induction (cylindrical) electrode and finally formulated into a

mathematical model. Marchant and Green (1982) come up with the idea of earthing the electrodes to avoid the short circuiting of power supply caused due to the wetting of electrodes (charged droplets may attracted back to the electrode). They used an oval shape electrode made of 5 mm thick wire, with major diameter 40 mm and minor diameter 19 mm. Maynagh *et al.* (2009) quantified the droplet charging characteristics of ring electrodes (radii: 10 and 15 mm) at varying voltage levels (1.5, 3, 5, and 7 kV), horizontal distances between the electrode and nozzle tip (1.5, 6, 10, and 15 mm), air flow speeds (14 $m \cdot s^{-1}$ to 23 $m \cdot s^{-1}$), and liquid flow rates (5, 12, and 25 $mL \cdot min^{-1}$). The highest charging was observed at a liquid flow rate of 5 $mL \cdot min^{-1}$, a voltage of 7 kV, and an air flow speed of 23 $m \cdot s^{-1}$, resulting in a current of 0.24 μA. Mamidi *et al*. (2013) achieved the electrification through a pure copper ring electrode (Teflon coating of 200 μm thickness) using positive high voltage based on electrostatic induction, while a stainless-steel electrode positioned behind the swirl disc serves as the ground. The electrode position from the nozzle were varied from 1 mm to 7 mm. Patel *et al.* (2013) studied different electrode material suitable for electrostatic spraying. The system incorporated electrodes made of Nickel (200/201 forged bar), Copper (98% pure), Stainless Steel (grade 304), Brass (70% Cu, 30% Zn), and Aluminum (98% pure), all embedded on an air-assisted nozzle cap. All the electrodes were capable of high voltage generation with the Nickel performed slightly better. The study employed the ring electrode configuration for all the materials selected. The electrodes with 22 mm peripheral diameter and 15 mm internal diameter was kept at 4 mm way from the nozzle tip with an applied voltage in the range of 0–3 kV. Jia *et al.* (2013) devised and subsequently put to the test an inductive electrostatic sprayer. The specific operational parameters were optimized as, electrostatic voltage – 20 kV, working pressure – 0.25 to 0.4 MPa, Charge to Mass Ratio (CMR) – 0.95 $mC \cdot Kg^{-1}$. The deposition rate was found to be 14 per cent higher than under uncharged droplets. Khatawkar (2019) employed an embedded ring electrode made of copper (5 mm thickness) with an internal diameter of 54 mm.

The studies concluded that, the current imposed on the spray cloud is directly related to the flow rate and applied voltage and inversely proportional to the liquid-filming characteristics and coaxial geometry of nozzle (inverse logarithmic manner).

Faster air speed positively influenced droplet charging, and a smaller electrode diameter led to reduced charge induction on the droplets. The quantity of droplet charging initially increased with greater distance between the ring electrode and nozzle tip but eventually either decreased or remained stable.

Anantheswaran and Law, 1979 devised an electrostatic spray charging system operated on a 12 V DC battery, with an output voltage ranged from 0 to -30 kV in 10 kV increments. Mamidi *et al.* (2013) utilizes a programmable 10 W high voltage module (EMCO High Voltage Corporation, Model No: F101) ranging from 0 to 10 kV. Jia *et al.* (2013) developed an inductive electrostatic sprayer with a charge-to-mass ratio of 0.951 $mC \cdot Kg^{-1}$ at 20 kV electrostatic voltage and 0.25 to 0.4 MPa working pressure. Charged droplets exhibited 14% higher deposition on the back side of the leaf compared to uncharged droplets. Martin and Latheef (2017) applied voltages in the range of 1-10 kV and observed a gradual rise in chargeability as the applied voltage increased, reaching the maximum charge-to-mass ratio of 1.686 $mC \cdot kg^{-1}$ at the highest applied voltage of 10 kV. Patel *et al.* (2017) were able to achieve an electrification over 10 $mC \cdot kg^{-1}$ at a charging voltage below 2.5 kV, with a liquid flow rate of 150 $mL \cdot min^{-1}$ and electric power consumption below 75 mW. There's a notable 2 to 3 times increase in liquid deposition, improving uniformity on both front and obscured targets. Patel *et al.* (2019) employed a electrostatic charging conditions of 1.5 kV applied voltage with a CMR exceeding 8 $mC \cdot kg^{-1}$, flow rate 110 $mL \cdot min^{-1}$, and 40 psi air pressure, surpassing the necessary threshold for achieving the wraparound effect. Assunção *et al*., (2020) designed a tractor (85 hp) operated hydraulic boom sprayer with a 12 m-boom, 24 nozzles spaced at 0.5 m intervals, and a 400 L tank capacity, operated at a pressure of 300 kPa with a voltage of 6.95 kV. Khatawkar *et al.* (2021) developed an electrostatic induction spray charging system integrated into a powered knapsack mist blower powered by a 6 V DC battery. The system was found working well with a highest CMR value of 1.088 $mC \cdot kg^{-1}$ at 5 kV electrode voltage and a 5 mm electrode placement position. Dai *et al*. (2022) used a high-voltage generator, operating at an input voltage of 220 V and offering an output voltage range of 0–20 kV, supplies the necessary electrostatic charge for the nozzle.

The air assisted electrostatic sprayer system developed by Celen *et al*., (2009) comprises of Lechler 110 - 02 spray nozzles at 2 bar pressure and a flow rate of 0.65 $L \cdot min^{-1}$. Air, generated by a 710 mm diameter fan with an airflow rate of 600 $L \cdot min^{-1}$ and a velocity of 36 $m \cdot s^{-1}$, is directed through pipes. Air nozzles aligned with spray nozzles release air at 5.6 $m \cdot s^{-1}$. Maynagh *et al*. (2009) observed that the optimal droplet charging occurs at a 5 $mL \cdot min^{-1}$ flow rate, 7 kV voltage, and 23 $m \cdot s^{-1}$ air flow speed, resulting in a current of 0.24 µA with a mean CMR of 1.032 $\mu C \cdot g^{-1}$. Mamidi *et al.* (2013) developed a manual hand pressure knapsack spray pump with a pressure range of 0 to 35 psi pressurizes the liquid for spraying. Khatawkar *et al.* (2021) observed the optimized the nozzle flow rate as 90 $mL \cdot min^{-1}$ at an operating pressure of 250-300 kPa. Dai *et al*., (2022) regulated the liquid flow rate as 0–5 $L \cdot min^{-1}$and pressure as 0– 6.9 bar for the electrostatic nozzle.

### 2.4.4 Measurement of charge to mass ratio (CMR)

The Charge-to-Mass Ratio (CMR) is the most pivotal parameter essential for the accurate prediction of the behavior of charged droplets when subjected to electrical, inertial, and gravitational forces.

Asano (1986) studied different techniques to measure droplet charges. Initially, an AC high voltage method was utilized, involving parallel plates and a power supply. Droplet trajectories between the plates were photographed, enabling the calculation of both charge and mass. The second method utilized a Faraday cage, incorporating a mesh screen to prevent ion current from the atomizing cup. Results revealed that the second approach (average CMR–$2.9 \times 10^{-2}$ $C \cdot kg^{-1}$) appeared more reliable than the first, as it accounted for the ion current from the cup, resulting in a more accurate assessment of the effective current.

The Faraday cage system of droplet cloud charge measurement system majorly consisted of a Faraday cage and provision for charge measurements. The Faraday cage was fabricated according to the specific requirements. The cage was grounded through the charge measurement unit mostly a multimeter and the electrostatic nozzle is positioned at the centerline of the cage. Before commencement of experiment, the

sprayer was operated at full throttle for some time (15 seconds: Sasaki *et al.*, 2013; 5 seconds: Assunção *et al*., 2020), allowing the equipment to stabilize before initiating spraying. During the experiments, the contact of charged droplets onto the of the Faraday Cage, and the subsequent transfer of the charge to the earth, generated an electrical current (Patel *et al*., 2017). The charged liquid spray was collected at a specific time (1 minute: Assunção *et al.*, 2020) and weighed. The spray current was then divided by the mass flow rate to determine the charge-to-mass ratio.

Maynagh *et al.,* (2009) evaluated the CMR using Faraday cage system, under controlled conditions, with varying parameters such as voltage (1.5, 3, 5, and 7 kV), air flow speed (14, 14.9, 17, 20.2, 21.6, and 23 $m \cdot s^{-1}$), charging electrode radii (10 and 15 millimeters), horizontal distances between the electrode and nozzle tip (1.5, 6, 10, and 15 millimeters), and liquid flow rates (5, 12, and 25 milliliters per minute). The study concluded that, higher voltages, faster air speeds have a positive impact on charging. Smaller electrode radii induce less charge. The droplet charging was initially rising with increased distance, then stabilized or decreased. Sasaki *et al.* (2013) assessed the spray cloud charge a multimeter (model ET-2510) with an accuracy of ± 1%. The experiments were conducted at varying spraying distances (0, 1, 2, 3, 4, and 5 m) from the Faraday Cage.

Patel *et al.* (2017) fabricated a Faraday cage using wire meshes and was connected to the earth potential through a digital multi-meter (Model No. 6514, Keithley). The dimensions of the cage were 60 x 30 x 30 cm. The Faraday cage apparatus designed by Marchewicz *et al*. (2019) comprising a two-layer grid of dense copper mesh with an inner diameter of 210 mm. The cage, suspended on dielectric threads to prevent leakage current, was positioned to allow the entire spray cone to flow into it. The results shows that the specific charge of droplets increases is directly related to the applied voltage on the induction electrode, up to a certain voltage magnitude. Beyond that point, the specific charge characteristic deviates from a linear relationship.

Assunção *et al*., (2020) constructed a Faraday cage with a cylindrical structure wrapped in metallic gauze (0.8 m in diameter and 0.6 m in length and 3.033 mm

aperture). A wooden rod ensured electrical isolation, and a multimeter connected to the cage and earthed. Dai *et al*. (2022) fabricated assessed the droplet charge using Faraday cylinder, digital multimeter (Fluke 8808A), and an electronic balance for weighing the droplets. The experiments were carried out at five levels of air and liquid pressure, with the size test additionally including five applied voltage levels. The charge-to-mass ratio test examines eight voltage levels to understand the impact on droplet charging.

### 2.4.5 Measurement of spray deposition

The spray deposition characteristics were assessed by spraying a liquid mixed with suitable tracer to a natural or artificial targets (Asano, 1986; Zhou and He, 2010) under either laboratory condition of field condition. The spray deposition was collected by means of different sampling techniques (chromatographic paper, petri dishes, filter paper, water-sensitive papers etc.) from both abaxial and adaxial surfaces and also at different leaf levels (top, middle, and bottom) along with monitoring the environmental parameters, including humidity, temperature, and wind speed (Celen *et al*., 2009; Miller, 2003). Adequate number of sampling surfaces can be placed based on the research requirements. Colorimetric methods were used to measure the tracer's concentration.

The generally used tracers are acid blue No. 9 at 0.5% (Asano, 1986) Tartrazine dye (Celen *et al.*, 2009; Barbosa *et al*., 2009) and Food, Drugs and Cosmetics dyes (FD&C) Blue No.1 (Sasaki *et al.*, 2013). Whereas, several studies also employed fluorescent dyes including Methylene Blue, Brilliant Sulpho Flavine (BSF), Rhodamine B (Zhou and He, 2010; Jia *et al.*, 2013; Khatawkar, 2019).

Asano (1986) and Zhou and He (2010) used a pseudo-plant made of metal and mirror-coated paper. The deposition rate is gauged using image-processing systems (Luzex 450 and Pax 4000). Barbosa *et al.* (2009) used artificial mylar cards for the determination of canopy penetration of different sprays in soybean (Glycine Max-L). Celen *et al.* (2009) evaluated the samplings from 27 different spot (filter paper). Sixteen additional filter papers were positioned around 300 mm from the tunnel to evaluate spray amounts outside the canopy. Leaf Area Index (LAI) of 75 leaves were done using a leaf area meter. Leaf density measurements gauged leaf distribution across plant

regions. Assunção *et al*. (2020) placed petri dishes around each experimental plot to estimate spray solution losses to the soil.

Zhou and He (2010) used water-sensitive papers and fluorescent tracer (BSF) mixed in tap water. The measurements were taken from different heights (top: 65 cm, middle: 40 cm, and bottom: 20 cm). At each height, four samples (two upper and two underside) were arranged systematically to prevent overlapping. In the laboratory, the samples underwent a washing process with 10 mL of distilled water, with the plastic bags shaken for 10 minutes using a mechanical shaker. The concentrations of the tracer were then determined using a luminescence spectrometer (model LS-55, Perkin-Elmer, Germany). The expression of spray deposits was in terms of $\mu g \cdot cm^{-2}$. Jia *et al*. (2013) analysed the fluorescent tracer solution using a spectrophotometer. Sasaki *et al*. (2013) made spray solution by mixing the dye in distilled water and absorbance was measured using a Biospectro spectrophotometer, model SP-22, which was properly calibrated for absorbance readings at 630 nm. Additionally, the calibration curve of the standard solution was generated using absorbance values. After the sprayings, the labeled items were enclosed in plastic bags, and 50 mL of distilled water were added and agitated for 30 seconds. Pascuzzi and Cerruto (2015) washed each sampled leaf with 50 mL of distilled water, and the absorbance of the resulting washing mixture was assessed using a spectrophotometer at a wavelength of 426 nm. Additionally, 10 leaves without treatment were randomly selected from the experimental plots before the tests to assess the background deposit. Assunção *et al*. (2020) assessed of deposition on maize plants using a bright-blue tracer (food colouring) at a dose of 400 $g \cdot ha^{-1}$ and the tracer was detected by absorbance using a spectrophotometer.

### 2.4.6 Measurement of spray droplet spectrum

Jahannama *et al.* (1999) utilized a Malvern 2600 Laser Scattering instrument to measure droplet sizes in both horizontal and vertical traverse to measure droplet sizes of a two-fluid concentric internal mixing induction charging nozzle. The experiments were carried out at three different operating pressures (0.14, 0.21, and 0.28 MPa) and specific spray liquid and air velocities (3 $m \cdot s^{-1}$ and 30 $m \cdot s^{-1}$, respectively). The study

concluded that the charged spray (40 to 75 μm) exhibited larger Volume Median Diameters (VMD) compared to the uncharged spray (12 to 32 μm).

Fritz *et al*. (2009) investigated the droplet spectrum using WSPs (Spraying Systems, Wheaton, Ill.) of size 26 x 76 mm. WSPs were arranged on a suspended table surface. After the treatment, WSPs were scanned using Droplet-ScanR (Version 2.2) software to analyze Volume Median Diameter (VMD) and Number Median Diameter (NMD). The results indicated an increase in droplet size (from 249 μm to 602 μm VMD) at higher application rates, attributed to overlapping in the range of 47–87 per cent. Maski and Durairaj (2010) studied spray deposition by fluorescent tracer technique and expressed as a normalized median diameter (NMD) range of 101–71 mm. Deposition of sprayed particles increased with charging (0 to 5.5 $mC \cdot kg^{-1}$) on the leaf abaxial surface and decreased with charging on the adaxial surface. Optimal results were observed at medium application speed with higher charging voltage.

Droplet spectrum study using Water-sensitive papers (WSPs) include strategically arranging them at various locations and heights (both on the front and back sides of the leaves) along the field of measurement. After the treatment, these WSPs were collected in separate labeled plastic bags and analysed using suitable techniques to obtain the droplet spectrum including VMD and NMD. Mishra *et al*. (2014) analysed the droplet spectrum using a system consisted of a Stereo zoom microscope with CCD camera (Make Radical Scientific Equipments), PC and monitor to control the analyzed image. USB digital scale software was used in laboratory to analyze the droplet on water sensitive paper strips. Patel *et al*. (2017) utilised WSPs for the study of an electrostatic sprayer on cotton plants. To ensure accuracy, adequate time (20 minutes after spraying) was allotted after each treatment for the spray material to descend, and for the material deposited on the water-sensitive papers (WSPs) to dry. In the laboratory, the analysis was done using a droplet analyser equipped with software called 'USB Digital Scale,' comprising a microscope, CCD camera, PC, and monitor for image control. Additionally, WSPs were analyzed using ImageJ, a java-based image processing scanning program known as the ‘DropletScan’ scanner-based system, which rapidly evaluates spray deposit distribution on water-sensitive paper

Dai *et al.* (2022) measured the droplet size of an electrostatic spray system using a laser particle size analyzer (OMEC DP-02, with a measurement range spanning 0.5–1500 μm). The air-assisted electrostatic nozzle is positioned between the collimated laser generator and the signal acquisition device through an insulated rod. The nozzle is situated 0.8 m away from the laser beam, guaranteeing that the discharged droplet cloud intersects the laser beam from the particle size analyzer in the same horizontal plane. The laser particle size analyzer facilitates the measurement of droplet size and distribution parameters of the air-assisted spray nozzle, including DV10, DV50 (VMD), and DV90.

## 2.5 TECHNOLOGIES FOR GENERATION OF HIGH VOLTAGE DC

Erwin Otto Marx in 1932 developed the Marx Principle, which involves generating a high voltage pulse by employing multiple capacitors in parallel for charging during the on-time and subsequently connecting them in series to achieve a higher voltage during the off-period (Dwivedi and Daigvane, 2010). Patel *et al*. (2014) proposed a new solid state Marx generator circuit with higher efficiency and pulse repetition rate. The goal was achieved by using solid state switches like IGBTs (Insulated-Gate Bipolar Transistor) and MOSFETs (Metal Oxide Semiconductor Field Effect Transistor) in the sphere gap assembly of conventional Marx generator *i.e*., each Marx stage includes a capacitor/pulse forming network and a high voltage switch.

Thummala *et al*. (2014) and Thummala *et al*. (2016) came up with a bidirectional DC-DC flyback converter capable of handling low input voltage (24 V) while providing a variable high output voltage (0–2.5 kV) to drive the capacitive actuator. The incremental actuator comprises three electrically isolated but mechanically connected capacitive actuators, necessitating three bidirectional DC-DC converters with high voltages (2-2.5 kV) for achieving incremental motion through the charging and discharging of the capacitive actuators. The prototype with a 4 kV MOSFET demonstrated an 89% charge energy efficiency in charging the capacitive load from 0 V to 2.5 kV and an 84% discharge energy efficiency in discharging it from 2.5 kV to 0 V, respectively.

Waluyo *et al*. (2015) employed modified Cockcroft-Walton voltage multiplier (CWVM) with up to four stages. The system utilized a regulated AC single-phase supply ranging from 0 to 220 V at 50 Hz, fed into a low voltage isolating transformer. Bhonde *et al*. (2017) generated a high voltage up to 5 kV DC from a 230 V, 50 Hz AC supply using a 8-stage CWVM, featuring a simple voltage multiplier circuit using diodes and capacitors. Nishanth and Karpagavalli (2019) developed a hybrid high voltage converter system consists of bi fly-back transformer whose secondary coils are connected to diode (3 nos) – capacitor (2 nos). The fly-back helps to reduce the voltage spikes in the primary side and improved the quality of the input voltage in the transformer. The hybrid converter achieved a fivefold gain while concurrently minimizing voltage distortion.

Tarigan *et al*. (2019) developed a HVDC system consists of a low voltage and high voltage. For low voltage system had a 12 Volt 5 Ampere transformer (Travo), a 5 A rectifier, an MC44603 A oscillator, and a MOSFET IGBT 20N60 for switching. High voltage was supplied by a 300 V power source, DD HS-05 150 WY for the fly-back transformer, stainless steel for plate electrodes, and a 1N4407 diode. Adjusting the number of turns in the transformer's primary and secondary coils controls the high voltage output. The system was capable of operating at a frequency of 100 kHz, generating a maximum pulse voltage ($V_{max}$) of approximately 52.5 kV with pulsed electric field strength of 50 $kV \cdot cm^{-1}$.

Khatawkar (2019) and Lukose *et al*. (2021) employed a diode split flyback transformer and a MOSFET for the high voltage generation. When the MOSFET switch was in the closed (ON) position, current flowed through the primary winding of the transformer, creating a magnetic field, that stores the energy. A diode connected in series with the secondary winding prevents the formation of secondary output current, allowing the electric current in the primary to gradually increase over time, storing energy. In the open position (OFF) of the switch, the magnetic field collapsed, and the stored energy was transferred to the secondary winding and ultimately to the load. Kenfack *et al*. (2022) The generation of HVDC with eight stage CWVM, which yielded up to 4.4 kV DC from an input voltage of 230 V, 50 Hz AC supply.

## 2.6 BIOLOGICAL EFFICACY OF ELECTROSTATIC SPRAYERS

Hislop *et al*. (1983) assessed the disease control effectiveness of hydraulic and experimental electrostatic nozzles on barley and wheat crops by spraying with oil and aqueous solutions mixed fluorescent tracers. The percentage of leaf area infected by diseases and the percentage of green leaf area were recorded at appropriate intervals. The Micron Ulva spinning disc and 'Electrodyn' systems with air assistance performed well.

Arnold *et al.* (1984) determined the biological effectiveness of sprayers by the disease and management assessment, which was done by counting the insect population on plants before and after spraying. The insect population on 10 plants per experimental plot was measured at 3, 13, 20, 27, 34, 41 and 48 days after the application of the insecticides. The study also analysed the spray deposition by collecting plant sample (after spraying) and extracting the tracer or insecticides by shaking the sample for 30 minutes in 100 mL methanol and then dried using anhydrous sodium sulphate. It was then analysed with gas chromatography. Phillips *et al*. (1988) conducted fungicide trials of an electrostatic sprayer with and without a charge. Fungicide (Propiconazole), was applied at both the full and one-third of the recommended rates. Disease and green leaf area assessments were conducted using ADAS keys at growth stage 71. Yield measurements were also recorded.

Kabashima *et al*. (1995) randomly collected 40 plant samples (1-inch diameter leaf punches) after treatment and sealed in jar and refrigerated until analysis within 24 hours. The sample collection was done at 1$^{st}$, 3$^{rd}$, 7$^{th}$, and 14$^{th}$ day after the application of insecticide, which was later extracted and analysed by means of a Hewlett-Packard gas chromatograph. The insect control was determined by counting the numbers of insect 4 days after the application. Narang *et al*. (2015) counted the pest on a total of three leaves per plant from a total of 10 randomly selected plants. The observations were made on both the upper and lower sides before and after the spray application. The pest count was then recorded on the 1$^{st}$, 3$^{rd}$, 7$^{th}$, and 10$^{th}$ days after the spraying. The percentage reduction of pests was determined by noting the difference in the number of

pests before and after the spray. Patel *et al*. (2016b) monitored both the disease control and pest mortality on cotton plants. Spraying trials were conducted on field plots measuring 50×20 $m^2$. The pest mortality was gauged by counting the number of pests (whitefly populations) on randomly selected 10 plants in the field and the observations were made before 10 am at intervals of 3, 7, and 15 days after the spray.